A brute-force spectral approach for wave estimation using measured vessel responses

Ulrik D. Nielsen[a,b], Astrid H. Brodtkorb[b], Asgeir J. Sørensen[b]

[a] *DTU Mechanical Engineering, Technical University of Denmark, DK-2800 Kgs. Lyngby, Denmark*
[b] *Centre for Autonomous Marine Operations, AMOS-NTNU, NO-7491 Trondheim, Norway*

Abstract

The article introduces a spectral procedure for sea state estimation based on measurements of motion responses of a ship in a short-crested seaway. The procedure relies fundamentally on the wave buoy analogy, but the wave spectrum estimate is obtained in a direct - brute-force - approach, and the procedure is simple in its mathematical formulation. The actual formulation is extending another recent work by including vessel advance speed and short-crested seas. Due to its simplicity, the procedure is computationally efficient, providing wave spectrum estimates in the order of a few seconds, and the estimation procedure will therefore be appealing to applications related to realtime, onboard control and decision support systems for safe and efficient marine operations. The procedure's performance is evaluated by use of numerical simulation of motion measurements, and it is shown that accurate wave spectrum estimates can be obtained for all wave directions in short-crested waves, taking the wave system to be composed by both wind generated sea and swell.

Keywords:
Wave spectrum, shipboard estimation, vessel responses, wave buoy analogy, Doppler Shift, spectrum transformation

1. Introduction

The level of autonomy in many aspects of marine operations, including shipping, is increasing, and the trend is believed to continue in the future [1, 2, 3]. One area of autonomy is in this context related to the risk and/or the performance evaluation of the actual operation, where focus may be on, say, cargo and passenger safety on a ship navigating in a seaway, hull girder integrity, fuel performance of the operating marine vessel, exact positioning and deterministic motion prediction of an offshore installation craft, etc. Regardless the type of operation, or whether the concern is on *deterministic* or *statistical* evaluations [4, 5, 6], it will be of an advantage to possess knowledge about the on-site sea state. For instance, statistics of the wave-induced acceleration level at given positions on a cruise ship can be easily calculated for various combinations of advance speed and heading, relative to the incoming waves, if a seakeeping code is coupled with an estimate of the sea state. Hence, it is possible to suggest (or "automatically enforce") the optimum combination of speed and heading in a safety-performance context.

One means to rely on for obtaining an estimate of the sea state at a vessel's exact geographic position is that of the wave buoy analogy, where onboard sensor measurements of wave-induced motion responses are processed to yield the wave energy distribution of the encountered wave system [7, 8, 9, 10, 11, 12]. In the past, various mathematical formulations of the wave buoy analogy have been studied with a main categorisation into A) spectral (frequency-domain) approaches based on Bayesian modelling or parametric optimisation, or B) time-domain approaches based on Kalman filtering or (recursive) nonlinear least squares fitting; an overview of available procedures (A and B) has been given by Nielsen [13]. However, just recently, a new implementation of the wave buoy analogy has been suggested by Brodtkorb et al. [14]. Although the initial work is considering vessels without advance speed, as focus was on ships being dynamically positioned (DP), very promising results have been obtained from full-scale DP experiments assuming long-crested waves.

The present study is a continuation of [14], with the aim to generalise the implementation to include mea-

Email address: udn@mek.dtu.dk (Ulrik D. Nielsen)

surements from a ship with advance speed, *and* letting the seaway be represented by short-crested (directional) waves. It is a central property that the implementation relies on a rather direct or brute-force kind of (spectral) approach that allows for high computational efficiency. The particular approach has, as mentioned, proved so far to have good estimating performance. As such, the approach can therefore stand alone but, due to its high computational efficiency, it might also be used as an 'initial sea state estimator' that gives a starting guess for one of the more - mathematically complex and "consecrated" - sea state estimation techniques based on, say, Bayesian modelling or parametric optimisation [7, 8, 15, 11, 16, 17]. Two characteristics of the present, updated implementation are noteworthy: (1) the implementation is a spectral approach derived in the frequency domain, (2) the given solution applies (initially) to the *encounter*-frequency domain and, thus, a transformation to *absolute* (true) frequency domain is necessary. In its fundamentals, the mathematical formulation is similar to the work by Brodtkorb et al. [14], which also relies on a spectral, brute-force approach, but the details are quite different. The differences are consequences of the generalised setting of the present, updated formulation; taking the speed-of-advance problem *and* short-crested seas into account. Altogether, it means that the governing equations of the two implementations - present work vs. [14] - are the same, but the solution strategies are not. It should be suggested already at this stage to consult available literature on the (practical) complications involved for a ship advancing relative to the incident waves [18, 19, 20, 21].

The simplicity behind the studied procedure is considered as an advantage in relation to many parts of real-time shipboard decision support tools as well as control (DP) applications, where, for instance, advanced controller schemes used in hybrid or switching control algorithms rely on computationally efficient algorithms. Online sea state estimates from rapid schemes, can be used to manipulate parameters in the control law directly, or be input to performance monitoring functions and risk assessment models that choose the best algorithms available [14]. As a further but more general note on the computational efficiency of the present sea state estimation procedure, sea state updates can be made so fast that it will be possible to directly carry out probabilistic assessments of the outcome by integrating the estimation procedure with probabilistic software tools. To date, this has not been possible with the existing sea state procedures [e.g. 7, 8, 15, 11, 16, 17], because of computational times in the order of minutes rather than seconds as is the case for the present work.

The article is composed as follows: After the introduction, Section 2 outlines the theory in terms of the governing equations as well as the solution strategy that includes a subsequent post-process/analysis. The implementation has some restrictions, mentioned in Section 3 together with other practicalities and characteristics. The procedure's performance is investigated through a number of test cases consisting of (artificial) simulations of measurement data, Section 4, and the associated results and discussions are given in Section 5. Finally, Section 6 presents conclusions and suggests further work.

2. Theory

The wave-induced (motion) responses of a ship in an irregular, short-crested seaway are considered. It is assumed that the responses are linear with the incident waves, and the speed and (mean) heading of the vessel relative to the waves are U and $\chi \in [0, 360[$ deg., respectively, with $\chi = 180$ deg. being head sea. The wave energy is distributed according to a directional wave energy spectrum $S(\omega_0, \mu)$ where ω_0 is the *absolute* (wave) frequency and $\mu \in]-180, 180]$ deg. is the angle describing the directional variation of the spectral ordinate relative to an axis parallel with the vessel's centreline. For a given vessel speed, the set of wave frequency and relative heading implies a certain (and unique!) *encounter* frequency ω_e determined by the Doppler Shift,

$$\omega_e = \omega_0 - \omega_0^2 \psi, \; \psi = \frac{U}{g} \cos\chi \tag{1}$$

where g is the acceleration of gravity, and for convenience $\mu = 0$ deg.

The Doppler Shift expresses a mathematical/physical elementary, but it is important to realise that the practical complications related to the Doppler Shift is by no means straight-forward to handle for wave-induced responses of an advancing ship in a seaway, as also mentioned in various textbooks [e.g. 18, 19, 20]. This will be further elaborated on in the following subsections, where the governing equations are specified together with the solution approach, but, at first, a common understanding of *encounter domain* versus *absolute domain* is beneficial. The particular problem-settings imply a solution, i.e. the wave spectrum estimate, obtained in the encounter domain, which is a mapping of the absolute - and true - domain, for an advancing ship. Thus, it is understood that the 'encounter domain' is that one observed from the ship as it advances relative to the inertial frame used for describing the progressing waves.

On the other hand, the 'absolute domain' is the domain any fixed observer without advance speed, relative to the inertial frame, is in. Later, the solution strategy makes direct use of the work by Nielsen [21], which can also be consulted to gain additional insight on the mapping between encounter domain and absolute domain, and vice versa.

2.1. Spectral analysis and fundamental equations

The estimation problem is formulated in the frequency domain through spectral analysis. In principle, this requires data, and the underlying physical process(es), to be stationary in the stochastic sense. Obviously, a truly stationary condition rarely exists for a ship (advancing) in a seaway due to changes in operational and environmental parameters. In a time frame in the order of 15-30 minutes it is however often considered acceptable to take conditions to be stationary, and this assumption will be made throughout, without necessarily stating this at the relevant places.

The linear relationship between waves and wave-induced vessel responses (here only heave, roll and pitch are considered) is given by the complex-valued motion transfer functions* $X_i(\ldots)$, which can be calculated using hydrodynamic software (e.g. strip theory and panel codes) and/or obtained by measurements. In a short-crested, stationary seaway it holds that,

$$R_{ij}(\omega_e) = \int X_i(\omega_e, \mu+\chi)\overline{X_j(\omega_e, \mu+\chi)}S_e(\omega_e, \mu)d\mu \tag{2}$$

where $R_{ij}(\omega_e)$ is the complex-valued cross spectrum for a pair (i, j) taken among the heave (z), roll (ϕ), and pitch (θ) responses $i, j = \{z, \phi, \theta\}$; $\overline{X_j(\ldots)}$ is the complex conjugate of the transfer functions in heave, roll and pitch for wave heading $(\mu + \chi)$ relative to the single waves from direction μ. $S_e(\omega_e, \mu)$ is the wave spectrum ordinate as observed from the advancing ship; note that index 'e' is used to emphasise that the ordinate refers to the encounter domain. As an assumption, $S_e(\omega_e, \mu)$ is represented by the product between a point spectrum $E(\omega_e)$ and a directional spreading function $\varphi(\mu)$,

$$S_e(\omega_e, \mu) = E(\omega_e)\varphi(\mu) \tag{3}$$

*Note, complex-valued motion transfer functions and response amplitude operators (RAOs) are *not* the same, although the terms are sometimes referred to as having similar meanings. Strictly speaking, the RAO is the square of the modulus of $X_i(\ldots)$.

Consequently, Eq. (2) is rewritten,

$$R_{ij}(\omega_e) = E(\omega_e)\int X_i(\omega_e, \mu+\chi)\overline{X_j(\omega_e, \mu+\chi)}\varphi(\mu)d\mu \tag{4}$$

The spreading function [e.g. 18] is taken as

$$\begin{aligned}\varphi(\mu) =& A(s) \times \cos^{2s}\left(\frac{\mu}{2}\right), \\ A(s) =& K \cdot \frac{2^{2s-1}\Gamma^2(s+1)}{\pi\Gamma(2s+1)},\end{aligned} \tag{5}$$

where Γ denotes the Gamma function, and s is the spreading parameter. The spreading function is obliged to fulfill $\int_{\mu_1}^{\mu_2}\varphi(\mu)d\mu \equiv 1$ from which the value of K is determined for a given pair of directions (μ_1, μ_2) that confines the directional spreading. If $(\mu_1, \mu_2) = (-180, 180)$ deg., then $K = 1$.

The cross spectra $R_{ij}(\omega_e)$ can be calculated for sets (i, j) of response measurement time series by using a cross power spectral density function, e.g., `cpsd` in MATLAB®. An example of corresponding sets of cross spectra $R_{ij}(\omega_e)$ calculated from three measured time history recordings is shown in Figure 1 taken from Brodtkorb et al. [14]. From the plots/spectra it is observed that $R_{ij}(\omega_e)$ is complex-valued for $i \neq j$, and that corresponding cross-spectra pairs, or *off-diagonal* pairs, are complex conjugate, i.e. $\mathcal{I}m(R_{ij}) = -\mathcal{I}m(R_{ji})$, which is a property that can be used to infer about the incident wave direction as seen later. The individual off-diagonal complex-valued spectra in Figure 1 can be given as corresponding real-valued pairs of amplitude- and phase-spectra by simply calculating the modulus and phase, respectively, for each frequency component of a given off-diagonal spectrum. For instance, the amplitude spectrum of the coupled motion of heave and roll is,

$$|R_{z\phi}(\omega_e)| = \sqrt{[\mathcal{R}e(R_{z\phi}(\omega_e)]^2 + [\mathcal{I}m(R_{z\phi}(\omega_e)]^2} \tag{6}$$

and it is noted that the 'amplitude spectrum' has a similar meaning as the three diagonal spectra of heave, roll, and pitch, respectively, in Figure 1; namely, the amplitude spectrum represents the distribution of 'power' with frequency of the particular (coupled) motion component. Consequently, a total of six independent power (and three phase) spectra can be computed from the three measured motion components heave, roll, and pitch.

Rather than solving Eq. (4) with complex-valued spectra, it is decided (for numerical stability reasons) to solve the equation by introducing instead the six power

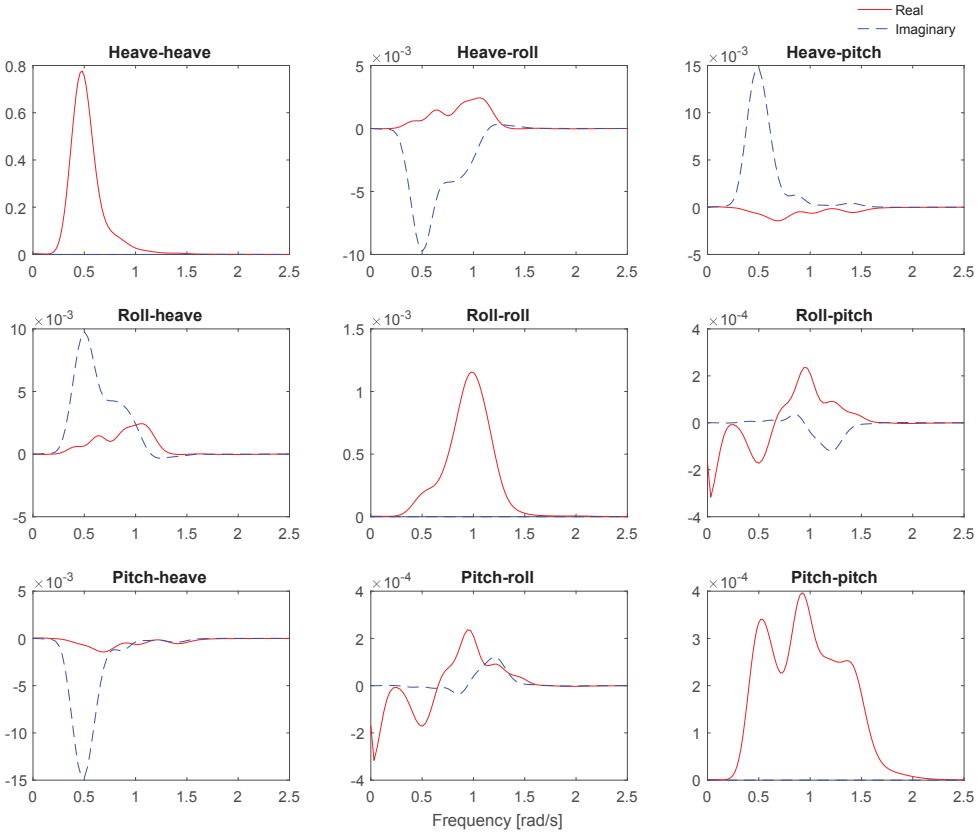

Figure 1: Cross spectra R_{ij} calculated from measured responses in heave [m], roll [rad.] and pitch [rad.] of the research vessel R/V Gunnerus. Brodtkorb et al. [14].

spectra, and to leave phase information/equations out in the first step. Thus, the six governing equations of the estimation problem read,

$$|R_{ij}(\omega_e)| = E(\omega_e) \int \left|X_i(\omega_e, \mu+\chi)\overline{X_j(\omega_e, \mu+\chi)}\right| \varphi(\mu) d\mu \tag{7}$$

formed by the pairs of motion components (i, j), which are (z, z), (ϕ, ϕ), (θ, θ), (z, ϕ), (z, θ), and (ϕ, θ). In Eq. (7), the left-hand side is obtained through measurements while the right-hand side is obtained through theoretical calculations combining available knowledge about the motion transfer functions together with information about the wave energy spectrum.

It is important to note that Eq. (7) is formulated in the encounter-frequency domain (ω_e). However, the motion transfer functions of a vessel are determined for a set of *absolute* wave frequencies (ω_0), and it is therefore necessary to introduce the Doppler Shift, Eq. (1), when solving Eq. (7) for the unknown point-wave energy spectrum $E(\omega_e)$. When a ship advances in following seas*, the Doppler Shift imposes a 1-to-3 mapping between encounter and absolute frequencies, since one encounter frequency may be "clocked" at three different absolute frequencies in certain conditions [21]. Turning to Eq. (7), this means that for any (discrete) encounter frequency - with the 'following sea conditions' fulfilled - the corresponding three absolute frequencies need to be simultaneously considered on the right-hand side of Eq. (7), as the assumption is that the three frequencies, i.e. wave components, will contribute "equally" to form the *encountered* wave component. Symbolically, the corresponding pairs of encounter and absolute frequencies are written as $\{\omega_e \rightleftarrows \omega_{01}\}$ and $\{\omega_e \rightleftarrows \omega_{01}, \omega_{02}, \omega_{03}\}$ for head seas and following seas, respectively; see Nielsen [21] for further details. The final version of the governing equation system is there-

*In this article, the term 'following seas' is at many places used to cover everything from following waves to beam waves (not included), while 'head seas' covers beam waves (included) to head waves.

fore given by,

$$|R_{ij}(\omega_e)| = E(\omega_e)\int |\Phi_{ij}(\omega_{01},\mu+\chi)|^2\varphi(\mu)d\mu \qquad (8)$$
$$+E(\omega_e)\int \left[|\Phi_{ij}(\omega_{02},\mu+\chi)|^2 + |\Phi_{ij}(\omega_{03},\mu+\chi)|^2\right]\varphi(\mu)d\mu$$

where $|\Phi_{ij}(\omega_{0k},\mu+\chi)|^2 = |X_i(\omega_{0k},\mu+\chi)\overline{X_j(\omega_{0k},\mu+\chi)}|$, and it is stressed that the first line of the equation is considered for all conditions, while the second line applies specifically to following seas. However, in following seas, the inclusion of the individual contributions is conditional, depending on the value of the encounter frequency relative to the wave heading and the speed of the vessel. A thorough discussion on these aspects is given by Nielsen [21]. As pointed out, the corresponding set of frequencies, encounter vs. absolute, is given by the Doppler Shift, and solving Eq. (1) for the absolute frequency yields for **head seas**,

$$\omega_{01} = \frac{1-\sqrt{1-4\psi\omega_e}}{2\psi}, \qquad \text{all } \omega_e \qquad (9)$$

and for **following seas**,

$$\omega_{01} = \frac{1-\sqrt{1-4\psi\omega_e}}{2\psi}, \qquad \omega_e < \frac{1}{4\psi} \qquad (10a)$$
$$\omega_{02} = \frac{1+\sqrt{1-4\psi\omega_e}}{2\psi}, \qquad \omega_e < \frac{1}{4\psi} \qquad (10b)$$
$$\omega_{03} = \frac{1+\sqrt{1+4\psi\omega_e}}{2\psi}, \qquad \text{all } \omega_e \qquad (10c)$$

2.2. Stepwise estimation of the wave spectrum

The speed-of-advance problem, introduced through the Doppler Shift, implies that the solution to Eq. (8) is obtained by considering head seas and following seas separately. Irrespectively, the *final* wave spectrum estimate is calculated in two steps: (i) an initial step concerned with the direct, or brute-force, solution of Eq. (8), and (ii) a second step concerned with a wave direction estimate computed through a post-processed solution. The practical details are outlined in the following but it is noteworthy that for the initial step (i) it is relevant only to consider relative wave headings just in the interval $\chi = [0, 180]$ deg., as the brute-force solution is concerned with an equation system, Eq. (8), formulated through power spectra. Thus, calculation of the right-hand side of Eq. (8) gives identical results for, say, $\chi = 70$ deg. and $\chi = 290$ deg. as these headings correspond to incident waves mirrored around the centreline of the ship ($\chi = 180$ deg. is incident waves head on).

(i) Brute-force solution

The brute-force solution does not assume a wave spectrum shape, or parameterise it in any way. Instead, the sea state estimate is based on the direct solution of the linear equation, Eq. (8), which is solved using an iterative scheme, as follows [14]:

$$\tilde{R}_{ij} = R_{ij}(\omega_e) - \hat{R}_{ij} \qquad (11a)$$
$$\hat{E}_{ij}(k) = \hat{E}_{ij}(k) + h\tilde{R}_{ij} \qquad (11b)$$
$$\hat{R}_{ij} = \hat{E}_{ij}(k)\int \sum_{m=1}^{3} |\Phi_{ij}(\omega_{0m},\mu+\chi_k)|^2\varphi(\mu)d\mu \qquad (11c)$$

performed for any pair (i, j) of motion components; herein taken as (z, z), (ϕ, ϕ), (θ, θ), (z, ϕ), (z, θ), and (ϕ, θ), and noting that Eq. (11c) is calculated conditionally with due account for head sea vs. following sea conditions, as addressed in relation with Eq. (8). Furthermore, it should be noted that Eq. (8) is solved for the entire range of (encounter) frequencies considered; in principle, in a frequency-by-frequency approach for the discrete computational settings, see below. Lastly, making a note of a more general character, the formulation of the problem in an iterative scheme, and based on a residual calculation, is a novel idea [14] compared to other existing spectral estimation procedures [e.g. 7, 8, 15, 11, 16, 17]. Indeed, the residual type of solution strategy is what makes the present procedure extremely efficient.

The practical implementation of the iterative scheme, or process, is illustrated using the pseudo script seen in Algorithm 1, which should be read with some supplementary remarks about:

- **Discretisation**. Wave directions and the set of encounter frequencies are discretised into N_χ and N_{ω_e} parts. Since the wave direction is unknown initially, a loop is made over all directions

$$\tilde{\chi}(k) = [0, 180] \text{ deg.}, \qquad k = 1 : N_\chi \qquad (12)$$

- **Initialisation**. The estimate of the (encounter) wave spectrum, and the estimate of the response spectrum are initially set to zero, $\hat{E}_{ij} = 0$ and $\hat{R}_{ij} = 0$. Compute the difference between the measured response spectrum and the estimated response spectrum $\tilde{R}_{ij} = R_{ij}(\omega_e) - \hat{R}_{ij}$.

- **Doppler Shift**. The given frequency is the encounter frequency ω_e, "produced" from the cross-spectral analysis, whereas the absolute frequency ω_0 will be a function of it. The function $f(\omega_e|\chi, U)$ is a result of the Doppler Shift; explicit expressions are seen in Eq. (9) and Eqs. (10a)-(10c).

- **Updates/adjustments**. Use $\tilde{R}_{ij}$ to make adjustments to $\hat{E}_{ij}$ with step size $h > 0$, and calculate the response spectrum estimate $\hat{R}_{ij}$ again. Do this until a threshold is reached $|\tilde{R}_{ij}| \leq \epsilon$, for $\epsilon > 0$.

The output from Algorithm 1 are six wave spectrum estimates per direction, yielding a spectrum estimate (block) matrix of dimension $6 \times (N_\chi \cdot N_{\omega_e})$,

$$\bar{E} = \begin{bmatrix} \hat{E}_{zz}(1,\omega_e) & \hat{E}_{zz}(2,\omega_e) & \dots & \hat{E}_{zz}(N_\chi,\omega_e) \\ \hat{E}_{\phi\phi}(1,\omega_e) & \hat{E}_{\phi\phi}(2,\omega_e) & \dots & \hat{E}_{\phi\phi}(N_\chi,\omega_e) \\ \hat{E}_{\theta\theta}(1,\omega_e) & \hat{E}_{\theta\theta}(2,\omega_e) & \dots & \hat{E}_{\theta\theta}(N_{\chi,\omega_e}) \\ \hat{E}_{z\phi}(1,\omega_e) & \hat{E}_{z\phi}(2,\omega_e) & \dots & \hat{E}_{z\phi}(N_\chi,\omega_e) \\ \hat{E}_{z\theta}(1,\omega_e) & \hat{E}_{z\theta}(2,\omega_e) & \dots & \hat{E}_{z\theta}(N_\chi,\omega_e) \\ \hat{E}_{\phi\theta}(1,\omega_e) & \hat{E}_{\phi\theta}(2,\omega_e) & \dots & \hat{E}_{\phi\theta}(N_\chi,\omega_e) \end{bmatrix} \tag{13}$$

noting that each component in Eq. (13) is a row vector of length N_{ω_e}, i.e. size $\left(\hat{E}_{ij}(k,\omega_e)\right) = 1 \times N_{\omega_e}$.

The matrix in Eq. (13) represents the brute-force solution to the wave estimation problem considered in Eq. (8). However, it is clear that the solution, as is, cannot be directly used, since 1) the solution is ambiguous with several sub-solutions (herein six) depending on the considered response, 2) no estimate of the wave direction, equivalently relative wave heading, is given as sub-solutions exist for all (specified) directions on a half circle [0,180] deg., and 3) the sub-solutions are encounter-wave spectra. Altogether, it is therefore necessary to post-process the brute-force solution, and the means for doing this are explained in the following.

(ii) Post-processed solution

The single wave spectrum estimates in Eq. (13) apply to the encounter domain and, hence, the estimates provide no information about the (true) distribution of wave energy in the absolute domain. Nonetheless, the spectra (Eq. 13) can be used to obtain an estimate of the total energy content of the wave system, since energy preserves irrespectively of the domain. In general, the total energy of a wave system can be given in terms of the significant wave height H_s, calculated from the area under the wave energy spectrum, see e.g. Eq. (22) in Subsection 4.2. Thus, the following $(6 \times N_\chi)$ matrix is obtained

$$\bar{H}_s = \begin{bmatrix} \hat{H}_{s,zz}(1) & \hat{H}_{s,zz}(2) & \dots & \hat{H}_{s,zz}(N_\chi) \\ \hat{H}_{s,\phi\phi}(1) & \hat{H}_{s,\phi\phi}(2) & \dots & \hat{H}_{s,\phi\phi}(N_\chi) \\ \hat{H}_{s,\theta\theta}(1) & \hat{H}_{s,\theta\theta}(2) & \dots & \hat{H}_{s,\theta\theta}(N_\chi) \\ \hat{H}_{s,z\phi}(1) & \hat{H}_{s,z\phi}(2) & \dots & \hat{H}_{s,z\phi}(N_\chi) \\ \hat{H}_{s,z\theta}(1) & \hat{H}_{s,z\theta}(2) & \dots & \hat{H}_{s,z\theta}(N_\chi) \\ \hat{H}_{s,\phi\theta}(1) & \hat{H}_{s,\phi\theta}(2) & \dots & \hat{H}_{s,\phi\theta}(N_\chi) \end{bmatrix} \tag{14}$$

where the single matrix elements are calculated by use of the individual components, i.e. $\hat{E}_{ij}(k,\omega_e)$, of Eq. (13).

In a perfect - purely theoretical - situation there will be one, and just one, column, say, no. k_K in Eq. (14), where all the (six) elements attain the same non-zero value; that is, the average of the values in the column is equal to the values of the single elements. Consequently, the hypothesis is that column no. k_K yields the optimum estimate of the significant wave height and, at the same time, the relative (mean) wave heading will be $\hat{\chi} = \tilde{\chi}(k_K)$, cf. Eq. (12). In practice, it is highly unlikely that the described "perfect" situation happens and, rather, the column (from Eq. 14) with the *smallest variation* in between the significant wave heights can be found. Thus, like for the purely theoretical situation, the given column, i.e. the discrete value of the heading representing the column, can be used as an estimate of the wave heading. In principle, this completes the estimation process, but it should be realised that, to this point, *six* wave spectrum estimates $\hat{E}_{ij}(k_K,\omega_e)$ apply to column k_K; i.e. one for each motion component, cf. Eq. (13). Therefore, the (final) optimum wave spectrum estimate is taken as the average of the six spectrum estimates; noting that the average is calculated frequency-wise,

$$\hat{E}_{final}(\omega_e) = \frac{1}{6}\Big(\hat{E}_{zz}(k_K,\omega_e) + \hat{E}_{\phi\phi}(k_K,\omega_e) + \hat{E}_{\theta\theta}(k_K,\omega_e) + \hat{E}_{z\phi}(k_K,\omega_e) + \hat{E}_{z\theta}(k_K,\omega_e) + \hat{E}_{\phi\theta}(k_K,\omega_e)\Big) \tag{15}$$

The estimation process is illustrated and explained with Figure 2. The two plots in the figure are the (initial brute-force) outcomes of the estimation procedure when it has been applied to artificially generated motion

Algorithm 1 Pseudo script for wave spectrum estimation

for $(i,j) = \{(z,z),(\phi,\phi),(\theta,\theta),(z,\phi),(z,\theta),(\phi,\theta)\}$ **do**
  for $k = 1 : N_\chi$ **do**
    $\hat{E}_{ij}(k) = zeros(1, N_{\omega_e})$
    $\hat{R}_{ij} = zeros(1, N_{\omega_e})$
    $\tilde{R}_{ij} = R_{ij}(\omega_e)$
    $\omega_0 = f(\omega_e|\chi, U)$
    while $|\tilde{R}_{ij}| > \epsilon$ **do**
      $\tilde{R}_{ij} = R_{ij}(\omega_e) - \hat{R}_{ij}$
      $\hat{E}_{ij}(k) = \hat{E}_{ij}(k) + h\tilde{R}_{ij}$
      $\hat{R}_{ij} = \hat{E}_{ij}(k) \int \sum_{m=1}^{3} |\Phi_{ij}(\omega_{0m}, \mu + \chi_k)|^2 \varphi(\mu) d\mu$
    end while
  end for N_χ
end for i

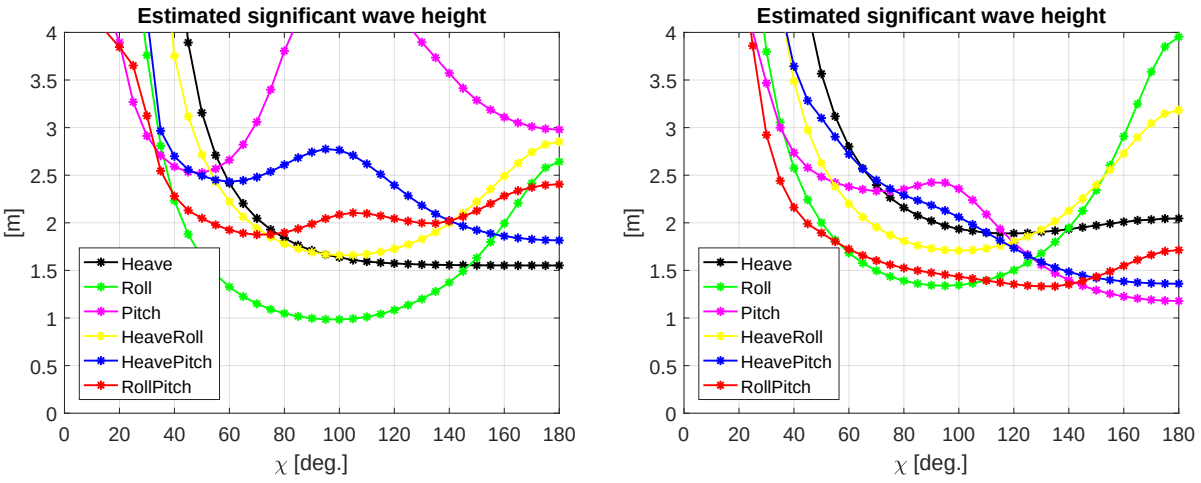

Figure 2: Variation of significant wave height H_s with mean relative wave heading χ using different motion components measured in a short-crested wave system. True parameters are for the left-side plot $\chi = 60$ deg. and $H_s = 2.0$ m, respectively, and for the right-side plot $\chi = 120$ deg. and $H_s = 2.0$ m.

data; the details about the vessel in study, about the time history generation, etc., are given later in Section 4, as the details are of minor importance for this explanatory example. In the given case (Fig. 2), two different sets of time history recordings of {heave,roll,pitch} are used as input to the estimation procedure. The two sets of motion recordings have been obtained/simulated using a short-crested wave system derived from the same type of wave spectrum; herein taken as a Bretschneider spectrum (see Sec. 4) with $H_s = 2.0$ m and $T_m = 6.5$ s. The only difference between the two sets of motion measurements is that the one set applies for a mean wave heading $\chi = 60$ deg. (left-side plot) and the other set for $\chi = 120$ deg. (right-side plot). In accordance with the selection process described above, it is found that the smallest variation between the estimated H_s-values is found for $\hat{\chi} = 55$ deg. and $\hat{\chi} = 125$ deg. for the left- and right-hand side plots, respectively. At these particular headings, the average significant wave heights are $\hat{H}_s = 2.2$ m ($\hat{\chi} = 55$ deg.) and $\hat{H}_s = 1.7$ m ($\hat{\chi} = 125$ deg.), as calculated from the two corresponding optimum wave spectrum estimates, cf. Eq. (15).

On a related note, the 'averaging-approach' has similarities to the study by Nielsen and Stredulinksy [22] that discusses the importance in selecting the best combination of motion measurements. This referred study uses also a mean-value-based solution, where all relevant combinations of motion measurements are considered and used for wave estimation. However, a general discussion about response selection for shipboard sea state estimation is beyond the scope of the present work and, thus, not addressed any further, but another useful study in this context has been given by Nielsen et al. [5].

It is a concern of the selection procedure described above that the obtained wave *heading* estimate will not necessarily be the (correct) optimum, since the selection procedure includes no distinction between incident waves on the port side and on the starboard side. The means to accommodate this problem is to make direct use of the complex-valued off-diagonal spectra, cf. Figure 1. Specifically, the imaginary parts of the off-diagonal elements should be considered, as these parts contain the necessary information because they are measures of the phases between the (coupled) motions. Hence, with reference to the fundamental equation, see Eq. (4), and the derived equation system Eq. (7) considering the six power spectra, three additional equations are considered:

$$\mathcal{I}m\left[R_{ij}(\omega_e)\right] = E(\omega_e)\int \mathcal{I}m\left[X_i(\omega_e,\mu+\chi)\overline{X_j(\omega_e,\mu+\chi)}\right]\varphi(\mu)d\mu \tag{16}$$

formed by the pairs of motion components (i, j), which in this case are (z,ϕ), (z,θ), and (ϕ,θ), respectively. Obviously, Eq. (16) needs to be implemented in the same way as Eq. (8), taking into account the practical complications in following sea. In contrast to the brute-force solution, cf. Algorithm 1, Eq. (16) is not solved for the point-wave spectrum $E(\omega_e)$ as the unknown, but for the wave heading instead. This is done by stepping through a discretised set of headings $\tilde{\chi}_\kappa$, $\kappa = 1, 2, ..., \varkappa$ on the

full circle [0,360[deg. and calculating, for each heading, the right-hand side of Eq. (16), using the optimum wave spectrum estimate given by Eq. (15). The calculated right-hand side of Eq. (16) can be subtracted from the left-hand side resulting in an error estimate ε_κ^2 for the particular heading $\tilde{\chi}_\kappa$. The error estimate is defined in the least squares sense using the L_2 norm, and the (final) optimum wave heading is thus found for the heading $\tilde{\chi}_\kappa$ where ε_κ^2 attains its minimum,

$$\min_{\tilde{\chi}_\kappa} \varepsilon_\kappa^2 \equiv \min \| \mathcal{I}m \left[R_{ij}(\omega_e) \right] - f(\tilde{\chi}_\kappa) \|^2 \qquad (17)$$

noting that the right-hand side of Eq. (16) has been written symbolically as $f(\tilde{\chi}_\kappa)$.

Clearly, the estimate of the optimum wave heading is made in a rather brute-force approach. This choice is made to keep the overall estimation procedure consistent and to be of a 'practical engineering' character, although it would be easy to obtain the optimum heading through a strict optimisation formulated through a cost function.

In a summarised form, the estimation process consists of the following points, focusing on the post-processed solution:

1. On the basis of the brute-force solution, i.e. from the block matrix in Eq. (13), calculate the corresponding matrix $\bar{H}_s$ of significant wave heights, cf. Eq. (14).
2. Find the column (k_K) in the matrix $\bar{H}_s$ that has the smallest standard deviation.
3. The six wave spectrum estimates of column k_K are used to determine the optimum (encounter) wave spectrum, calculated as the average of the six spectra in column k_K:

$$\hat{E}_{final}(\omega_e) = \frac{1}{6} \Big(\hat{E}_{zz}(k_K, \omega_e) + \hat{E}_{\phi\phi}(k_K, \omega_e) + \hat{E}_{\theta\theta}(k_K, \omega_e) + \hat{E}_{z\phi}(k_K, \omega_e) + \hat{E}_{z\theta}(k_K, \omega_e) + \hat{E}_{\phi\theta}(k_K, \omega_e) \Big) \qquad (18)$$

4. Apply the optimum wave spectrum $\hat{E}_{final}(\omega_e)$ to select the optimum wave heading by minimising the error between the left- and right-hand sides of Eq. (16).

2.3. Transformation to absolute domain

Altogether, the outlined estimation procedure results in a point-wave spectrum estimate *and* an estimate of the mean relative heading. The wave spectrum has been estimated for a (particular) set of *encounter* frequencies, and, hence, the significant wave height can be directly obtained from the spectrum. On the other hand, the spectrum reveals no explicit information about the absolute, or true, distribution of wave energy; or equivalently said, knowledge about characteristic *absolute* wave periods such as the mean period (T_m) and peak period (T_p) is unavailable if no action is taken. Consequently, it is needed to further process the solution and to *transform the spectrum from encounter to absolute domain*. Indeed, such a transformation procedure is available, since a dedicated study by Nielsen [21] on the topic/task has been conducted in parallel with the current work. The details of the transformation procedure will not be given here, and it suffices to say that spectrum transformation generally can be uniquely carried out when the ship sails "against" the waves (beam to head sea). In following sea conditions, however, there exists no unique solution to the problem. Instead, a reasonable approach valid for practical engineering must be applied, and the mentioned work [21] outlines one viable approach that can be used to transform a wave spectrum from encounter to absolute domain; which is exactly what is needed in the present study, where an encounter-wave spectrum is available together with knowledge about the relative wave heading. The final result from the estimation procedure is therefore obtained by transforming the optimum wave spectrum estimate $\hat{E}_{final}(\omega_e)$,

$$E(\omega_0) = g(\hat{E}_{final}(\omega_e) | \tilde{\chi}_\kappa, U) \qquad (19)$$

where $g(\ldots)$ is the mapping-function [21] which consistently transforms the estimated wave spectrum from encounter to absolute domain.

3. Practicalities

To this point the estimation procedure has been presented for its fundamental concepts and the associated equations. Thus, it remains as the main task to evaluate the procedure. The evaluation will be performed using perfectly controlled settings in terms of computational simulations. It is, however, important to touch upon some practical aspects of the estimation procedure before its performance is discussed, and these aspects are addressed in the following, where focus will be on limitations, spectral calculations, and on a ship's motion transfer functions and their use in the context of sea state estimation. Moreover, a very brief description of the central point(s) of the wave spectrum transformation algorithm [21] is included.

3.1. Limitations

Due to a solution strategy relying on a residual calculation through an iterative scheme, the estimation pro-

cedure provides a *point spectrum*; initially obtained in the encounter domain and subsequently transformed to the absolute domain with due account for vessel speed and (mean) wave direction. Described by a point spectrum, the wave system is inherently considered as unidirectional, but short-crested waves are "imposed" into the solution by an overlaid directional spreading function. Nonetheless, the solution, or the wave spectrum estimate, is restricted from handling truly crossed-sea conditions where wind waves from one direction occurs at the same time as swells from another (very) different direction. In short, the estimation procedure is limited to deal with mixed seas (wind waves + swells) from the same direction. Or, said equivalently, the procedure facilitates estimation of crossed-seas, but the final estimate will be given as a point spectrum* with no distinction between the directions.

It is considered a strength that the wave spectrum estimate - obtained in the initial study [14] made for ships without forward speed - is completely non-parametric, since typical pre-specified wave spectrum shapes (Bretschneider, JONSWAP, etc.) are not always appropriate. The brute-force and post-processed solution $E(\omega_e)$ obtained in the current, updated work considering vessels with advance speed is also non-parametric. However, the final - and transformed - wave spectrum $E(\omega_0)$ will be only partly non-parametric because the transformation algorithm [21] relies on a procedure introducing parametric wave spectrum shapes.

Like for all other shipboard estimation techniques, the current estimation procedure will be limited to estimate wave components at a certain frequency band. This limitation is due to the general characteristic of a ship being a low-pass filter. Hence, the algorithm will work best for wave lengths larger than some specific value relative to the ship length (and breadth); which obviously are case-specific parameters.

3.2. Spectral calculations

It has already been stressed that stationary conditions are considered/assumed exclusively in this study, which means that spectral analysis of the motion recordings, given as time series, will provide reliable results. In practice, it is difficult to define exactly when conditions are no longer (statistically) stationary, implying that any outcome from spectral analysis will be unreliable. Consequently, it should be interesting to consider, more carefully, in which conditions 'standard' spectral analysis cannot be applied for its particular purpose, i.e. to provide (cross) response spectra, in the context of shipboard sea state estimation. At the same time, it should be mentioned that elaborate means and procedures exist for conducting spectral analysis in nonstationary conditions and, potentially, it should therefore be possible to apply the studied (spectral) estimation procedure even when conditions are not stationary. However, these types of work are beyond the scope of the present study, and herein it suffices to note that several methods/tools are available to carry out the spectral analysis in case of stationary data. The present work uses a built-in function `cpsd` of MATLAB® which can readily be applied to any set of two time history recordings to produce the mutual set of cross-spectra, see Figure 1.

By nature, ocean wave spectra are smooth in their frequency-wise distribution (and as well in their directional-wise distribution), and it is therefore necessary to work with smoothed versions of the set of response spectra. In the numerical studies analysed later, smoothing is imposed by a Parzen window applied with a 50% overlap on the full range of frequencies from the FFT. The resulting spectra are specified on 600 frequencies for a set of lower and higher cut-off frequencies f_{low} = 0.0008 Hz and f_{high} = 1.0 Hz, respectively, and, consequently, the wave spectrum estimate(s) apply to the same range of encounter frequencies. Indeed, it is possible to work with such a fine frequency resolution only because of a highly computationally efficient estimation algorithm. In real-case practices, however, the resolution should be significantly lower in order to optimise computational speed; taking note that, at some point, the wave estimates will be affected if the resolution is too coarse.

3.3. Motion transfer functions

The performance evaluation of the estimation procedure is in this study made exclusively through computational simulation of motion measurements; using the same set of motion transfer functions to both *generate* the measurement time series and to subsequently *estimate* the wave spectrum. As a consequence, details about the transfer functions are of minor importance and just a few words are given here about the applied set of motion transfer functions.

Instead of using the transfer functions of the actual vessel, based on the detailed hull geometry, the transfer functions of a homogeneously loaded barge with the same main dimensions (length, breadth, draught) as the vessel are used in the estimation procedure. In this particular case, a set of closed-form expressions developed

*Likely, the wave spectrum estimate will be fairly accurate if the incident directions of wind waves and swells are not too different. A hypothesis, however, that needs attention in any future work.

by Jensen et al. [23], Mansour et al. [24] yields a good representation/approximation of the transfer functions considering heave, roll, and pitch. Of course, the transfer functions of the real hull geometry, obtained e.g. by strip theory or a panel code, could easily be applied in the sea state estimation algorithm instead of the closed-form expressions. However, the use of closed-form expressions offer a convenient - and highly computational efficient - way to deal with transfer functions in varying operational conditions without the need to interpolate.

3.4. Wave spectrum transformation algorithm

As has already been pointed out, the details of the wave spectrum transformation algorithm outlined in [21] will not be dealt with herein. Anyhow, a few remarks about the algorithm are noteworthy.

Briefly said, the algorithm is based on a scaling approach that assures preservation of energy at corresponding sets of encounter and (true) absolute frequencies. Thus, a set of scaling ratios apply to specific absolute frequencies, obtained through the Doppler Shift of given encounter frequencies, and multiplication between the scaling ratios and the *encounter* wave spectrum ordinate will make the transformed *absolute* wave spectrum available. It happens that spectral ordinates are erroneously transformed from the encounter domain to a high-frequency range of the absolute spectrum; despite 'consistent' multiplication with the spectral ratios. Consequently, the transformation algorithm introduces a tail-fitting which makes sure that for frequencies higher than a user-defined value, the tail of the transformed spectrum follows that of a Bretschneider spectrum. In the particular case studies presented later, this values is taken as 0.25 Hz.

4. Case studies using simulated measurements

The performance of the estimation procedure (Sec. 2) is evaluated using artificial time series data generated through computational simulations. In this setting, exact knowledge is available about the true wave energy spectrum and associated sea state parameters and, hence, it is easy to conduct comparative studies with the corresponding wave spectrum estimate obtained by the estimation procedure.

4.1. Vessel data

Time series simulations of the motion components {heave, roll, pitch} have been performed for an example ship* with data given in Table 1. The example ship was considered in the initial study [14] using DP full-scale data, and it is a scheduled task to also conduct sea state estimation analysis using full-scale data of the vessel at forward speed.

Table 1: Main particulars of the example ship and other necessary data used to calculate the (closed-form) transfer functions.

Length, L_{pp}	28.9 m
Breadth, B	9.6 m
Draught, T	2.7 m
Block coefficient, C_B	0.56 [-]
Waterplane coefficient, C_{WP}	0.84 [-]
Displacement (mass), Δ	417 000 kg
Transverse metacentric height, GM_T	2.66 m

4.2. Wave scenarios (test cases)

Various test cases form the background for the performance evaluation of the estimation procedure. Each test case is represented by a given short-crested input-wave system characterised by a parameterised wave energy spectrum and its associated (true) integrated wave parameters such as significant wave height H_s, mean (wave) period T_m, and peak (wave) period T_p. Thus, the wave elevation and corresponding motion records can easily be generated for a ship advancing in the particular wave system, see Subsection 4.3 below.

An overview of the test cases (A, B, C) is seen in Table 2 which specifies the (absolute) input-wave parameters together with other operational parameters. It is noteworthy that two of the main test cases, A and B, differ only by the selected advance speed being $U = 5.0$ knots and $U = 10.0$ knots, respectively. The actual wave system, on the other hand, is exactly the same for the two cases, and so is the selected sets of mean headings χ_0 relative to the wave system. The main purpose with the subcases of cases A and B is to evaluate the performance of the estimation procedure when the ship advances at different relative (mean) headings specified as $\chi_0 = \{0, 10, \ldots, 350\}$ deg. Notably, the concern is the procedure's ability to correctly estimate the wave system in following seas, and its ability to differentiate between incident waves on the starboard side or the port side. Note, at deep water conditions, the particular choice of mean period $T_m = 6.5$ s corresponds to an absolute wave length $\lambda = \frac{gT_m^2}{2\pi} = 66.0$ m, i.e. $\lambda/L_{pp} \approx 2$. Thus, the wave system is of a wave-length regime where most of the wave energy is concentrated at wave lengths inducing "reasonable" response levels of the considered motion components {heave, roll, pitch}, see Figure 3, which is of relevance due to a ship's inherent low-pass-

*The example ship is *R/V Gunnerus* which is owned and operated by NTNU.

Table 2: Summary of test cases using a Bretschneider wave spectrum overlaid with a spreading function, where the latter has $s = 4$ in every case.

Cases	U [knots]	$T_{m,0}$ [s]	$T_{p,0}$ [s]	$H_{s,0}$ [m]	χ_0 [deg.]
A	5.0	6.5	8.4	2.0	{0:10:350}
B	10.0	6.5	8.4	2.0	{0:10:350}
C	10.0	4.3+9.8 (6.1)	5.6+12.7	2.0+2.0 (2.8)	{0:10:350}

filtering characteristics. The reason to include two vessel speeds is that fewer waves will "overtake" the vessel for the higher vessel speed ($U = 10$ knots) compared to the lower one, when the ship advances in following seas, and this fact may influence the outcome from the estimation procedure, as the physics behind the 1-to-3 relationship is indeed governed by the advance speed of the vessel (together with wave heading).

In addition to cases A and B, one last test case, C, representing a double-peaked wave system, is used to test the estimation procedure's performance in sea states with swells and wind sea occurring at the same time.

The listed wave scenarios in Table 2 are described by a Bretschneider (point) wave spectrum $S_B(\omega_0)$ overlaid with a spreading function $\varphi(\mu)$ (Eq. 5). That is, for the generation of the wave elevation and the corresponding motion records, the input-wave spectrum $\hat{S}(\omega_0, \mu)$, also denoted the *generating spectrum*, is taken as:

$$\hat{S}(\omega_0, \mu) = S_B(\omega_0)\varphi(\mu) \tag{20}$$

$$S_B(\omega_0) = 173\frac{H_s^2}{T^4\omega_0^5}\exp\left[-\frac{692}{T^4\omega_0^4}\right] \tag{21}$$

where the characteristic period T depends on which statistical period is given. The following substitutions apply: $T = T_m$ for the mean period T_m, $T = 0.772T_p$ for the peak period T_p, or by $T = 1.086T_z$ for the zero-upcrossing period T_z. Case C will be taken as the sum of two Bretschneider spectra with parameters as given in Table 2.

The generating spectrum depends on the input parameters (e.g., H_s, T_m) and for quantitative comparisons it is relevant to obtain the corresponding estimates. Thus, integrated/estimated wave parameters can be derived from the n-th order spectral moments of a wave spectrum,

$$m_n = \int_0^\infty \omega_0^n E(\omega_0)d\omega_0 \tag{22}$$

$$H_s = 4\sqrt{m_0},\ T_m = 2\pi\sqrt{\frac{m_0}{m_1}},\ T_p = \frac{2\pi}{\omega_p} \tag{23}$$

where $E(\omega_0)$ is given by Eq. (19), and ω_p is the frequency corresponding to the spectrum peak.

4.3. Time history simulations

The wave elevation and the corresponding vessel motions are considered as Gaussian distributed. Hence, in linear, short-crested waves the time history record $R(t)$ of a wave-induced motion component can be generated using a set of uncorrelated, standard normal distributed variables u_{nm} and $\bar{u}_{nm}$ [e.g. 25],

$$R(t) = \sum_{n=1}^{N}\sum_{m=1}^{M}[u_{nm}c_{nm}(t) + \bar{u}_{nm}\bar{c}_{nm}(t)] \tag{24}$$

The deterministic coefficients $c_{nm}(t)$ and $\bar{c}_{nm}(t)$ are for an advancing vessel given by,

$$c_{nm}(t) = \sigma_{nm}|\Phi_R(\omega_{0,n}, \mu_m + \chi) \cdot |\cos\left(\omega_{e,nm}t + \epsilon_R(\omega_{0,n}, \mu_m + \chi)\right) \tag{25}$$

$$\bar{c}_{nm}(t) = -\sigma_{nm}|\Phi_R(\omega_{0,n}, \mu_m + \chi)| \cdot \sin\left(\omega_{e,nm}t + \epsilon_R(\omega_{0,n}, \mu_m + \chi)\right) \tag{26}$$

$$\sigma_{nm}^2 = \hat{S}(\omega_{0,n}, \mu_m)\Delta\omega_{0,n}\Delta\mu_m \tag{27}$$

where the modulus (amplitude) and the phase of the motion transfer function are
$|\Phi_R(\omega_{0,n}, \mu_m + \chi)|$ and $\epsilon_R(\omega_{0,n}, \mu_m + \chi)$, respectively, for the particular motion component R. The generating wave energy spectrum $\hat{S}(\omega_0, \mu)$ is discretised at N frequencies and M directions. The present formulation considers time histories of wave-induced motion components observed from the advancing vessel. This means that the encounter frequency ω_e, appearing in the deterministic coefficients, is given by, cf. Eq. (1)

$$\omega_e = \left|\omega_0 - \omega_0^2\psi\right|,\ \psi = \frac{U}{g}\cos\chi \tag{28}$$

for any absolute frequency ω_0.

Based on the parameters of a particular test case, see Table 2, 20 sets of wave and motion measurements are generated. The need for several corresponding records, here 20, of wave and motion components is due to the fact that a statistical evaluation of the estimation procedure's performance is necessary, since a single, finite time history recording is just one out of the infinitely many that comprise the "complete" ensemble. The single time history records are 20 minutes long and

made from $N = 800$ wave components spaced non-equidistantly on the frequency interval $]0, 2\pi]$ at $M = 19$ wave directions using the spreading function (Eq. 5) with $s = 4$. The time history simulations are generated at 10 Hz, and, after adding white noise (SNR = 20), the records are down-sampled to 2 Hz to artificially add measurement noise.

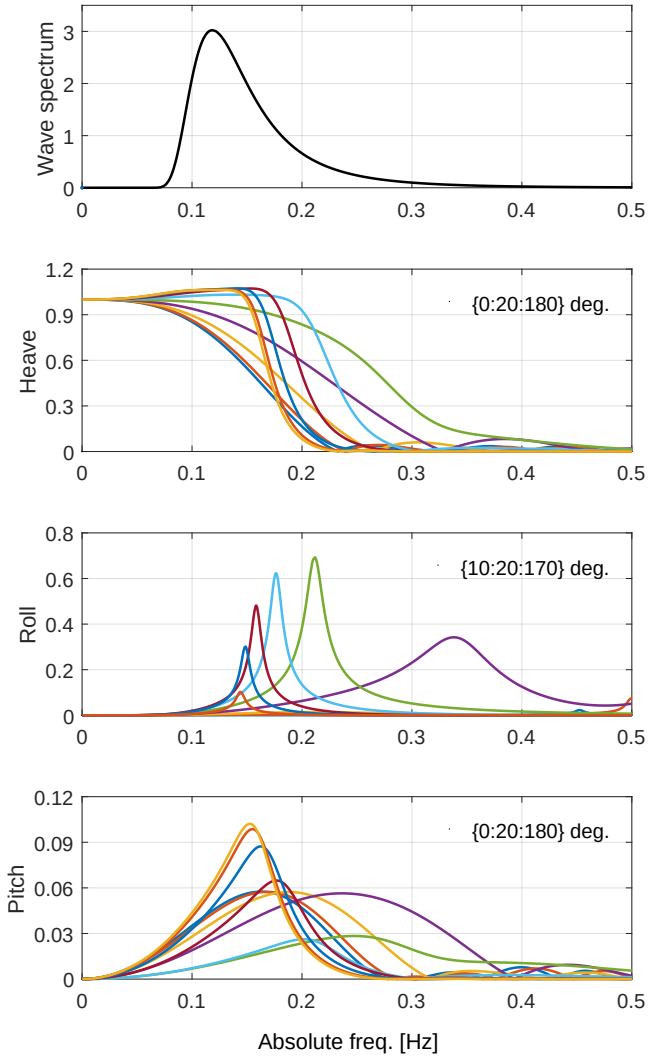

Figure 3: A Bretschneider wave spectrum (uppermost plot) with $T_m = 6.5$ s and $H_s = 2.0$ m is used as the generating spectrum for the time series simulations of {heave, roll, pitch} at forward speed $U = 10$ knots. The modulus (amplitudes) of the motion transfer functions are shown below the wave spectrum, and the results for different relative headings are presented, leaving the detailed legends out since the interest is merely the 'qualitative variation' between the different headings. Units: Wave spectrum [m^2s]; Heave [m/m]; Roll [rad/m]; Pitch [rad/m].

5. Results and discussions

In this section, the performance of the estimation procedure is analysed and discussed. The case studies, see Table 2, have been presented in the preceding section, and the result will simply be the outcome of the estimation procedure when it is applied to the test cases. However, two overall subsets of results are considered, with the main subset reported in the following subsection that studies a situation where perfect knowledge about the hydrodynamic behaviour of the vessel in waves exists. That is, a subset/situation where the motion transfer functions "by default" yield a perfect description of wave-vessel interactions. As another situation, incomplete knowledge about the wave-vessel interactions is introduced as a more realistic scenario. This situation can easily be studied by working with two different sets of motion transfer functions; one set for the time series generation and one set for the wave estimation process.

5.1. Perfect transfer functions

In this part of the evaluation of the estimation procedure, the same set of transfer functions is used for the motion generation/simulation and for the sea state estimation, respectively.

Cases A and B

The specific outcome of the estimation procedure is a (2D) wave spectrum $E(\omega_0)$, and two (arbitrary) selections of estimated spectra taken from cases A and B are shown in Figures 4 and 5, respectively.

In the figures, each plot relates to a specific *true* wave heading, shown in the title of the plot, and the *estimated* wave heading is printed in the plot's legend. It is noteworthy that any plot is the result of just one out of the 20 sets of time history simulations representing the individual subcases/headings reported in Table 2. As such, it should be remembered that the single spectrum estimate may actually be estimating nicely the realised wave elevation process, i.e. its associated energy spectrum, for the specific (stochastic) realisation, although the spectrum estimate and the true generating (deterministic) spectrum are not fully alike for the specific realisation. However, on average, and theoretically speaking, infinitely many realisations should have a mean process/spectrum that will exactly be represented by the (true) generating spectrum. In this study, 'infinitely many' is taken as 20 realisations.

From the plots in Figures 4 and 5, it is evident that there is a good agreement between the true generating spectrum and the estimated one, including wave heading, in all of the considered comparisons. Although this observation is not entirely representative to every single

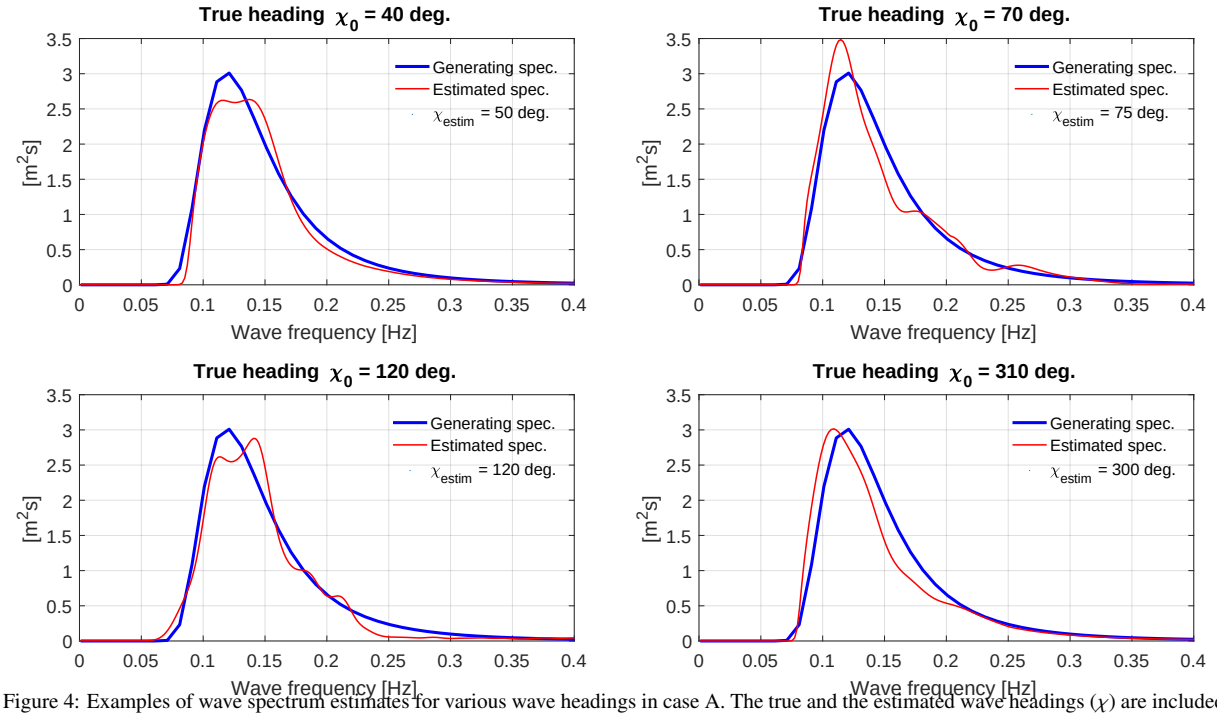

Figure 4: Examples of wave spectrum estimates for various wave headings in case A. The true and the estimated wave headings (χ) are included in the plot titles and legends, respectively.

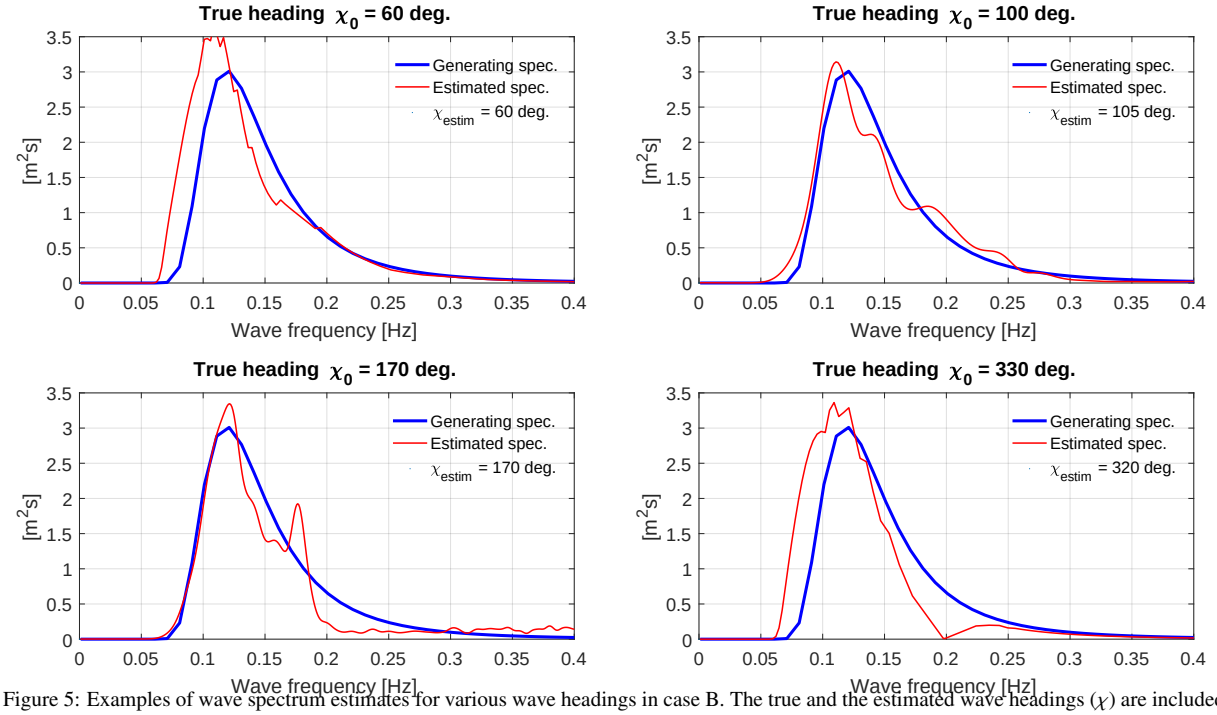

Figure 5: Examples of wave spectrum estimates for various wave headings in case B. The true and the estimated wave headings (χ) are included in the plot titles and legends, respectively.

set of time history recordings for every single (true) subcase of cases A and B, Table 2, the general picture observed from Figures 4 and 5 resembles the overall trend of the spectrum estimates very well.

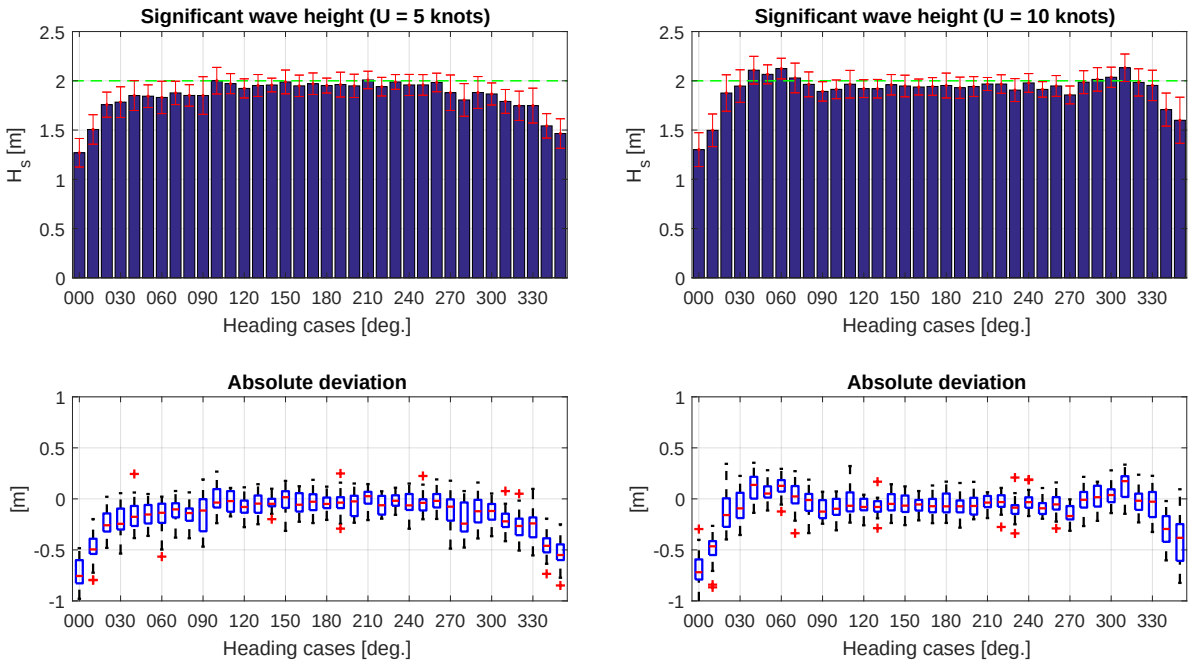

Figure 6: Upper plots: Estimates of **significant wave height** for all subcases (headings) of cases A (left-hand side) and B (right-hand side) with the true value indicated by the green dashed line. Lower plots: Deviations between estimates and true value shown as box plots. On each box, the central mark is the median, and the upper and lower edges of the box are the 25th and 75th percentiles, respectively. The whiskers extend to the most extreme data points which the algorithm considers not to be outliers, and the outliers are plotted individually.

The trend, or the statistics, of the entire set of outcomes for cases A and B can be seen in Figures 6-9. Basically, the four figures contain the same sort of statistical information but relevant for the significant wave height (Fig. 6), the mean period (Fig. 7), the peak period (Fig. 8), and the (mean) relative wave heading (Fig. 9), with results shown for both cases A and B as the left-hand side plots ($U = 5$ knots) and the right-hand side plots ($U = 10$ knots), respectively. The pairs of upper and lower plots in the figures present the same type of comparisons: The upper plot shows the average value of the outcome of estimates of the particular wave parameter considering all headings, and with the average value based on the 20 sets of simulations for each heading. The error bar on the top of each column indicates plus/minus the standard deviation. The lower plot shows the statistics* of the absolute deviation between estimates and the corresponding true value of the particular wave parameter. Irrespectively of the plot/figure it is decided to keep all comparative measures in absolute scale, since relative deviation/scale of wave parameters has, strictly speaking, only a meaning for the significant wave height; which is identical for cases A and B in this study.

Generally, the agreement (Figs. 6-9) between the estimates and the true values are good for all of the considered wave parameters, including the relative wave heading. Thus, it is observed that the average values (and the medians) are close to the true values, with small variations around them although 'outliers' occur here and there; and taking note that the peak period on average is estimated well but being the parameter with the most scatter in the results. The general agreement drops a bit, however, when the ship is exposed to following sea conditions at incident wave angles closely in line with the vessel's centreline ($\chi \approx 0 - 10$ deg. and $\chi \approx 350 - 360$ deg.).

Taking a more detailed look at the statistics, the results for the significant wave height (Fig. 6) reveal that the energy level rather consistently is slightly below the true level; an observation not limited to only following sea conditions. This sort of underestimation is a consequence of the filtering characteristic of a vessel in waves, making the ship less responsive to high-frequency waves, for what reason the observation/underestimation is expected. Indeed, this is one of the inherent and fundamental drawbacks of the wave buoy analogy and, as such, the observation applies to

*Herein, the built-in function `boxplot` of MATLAB® is used.

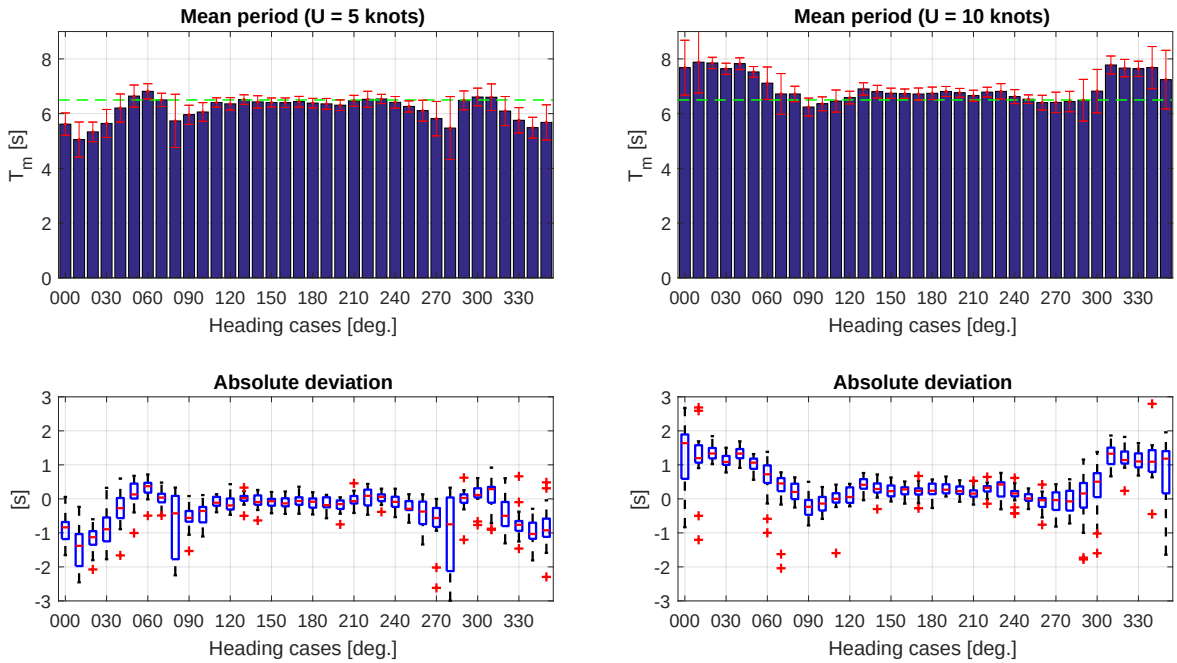

Figure 7: Upper plots: Estimates of **mean period** for all subcases (headings) of cases A (left-hand side) and B (right-hand side) with the true value indicated by the green dashed line. Lower plots: Deviations between estimates and true value shown as box plots; info is given in the caption of Fig. 6.

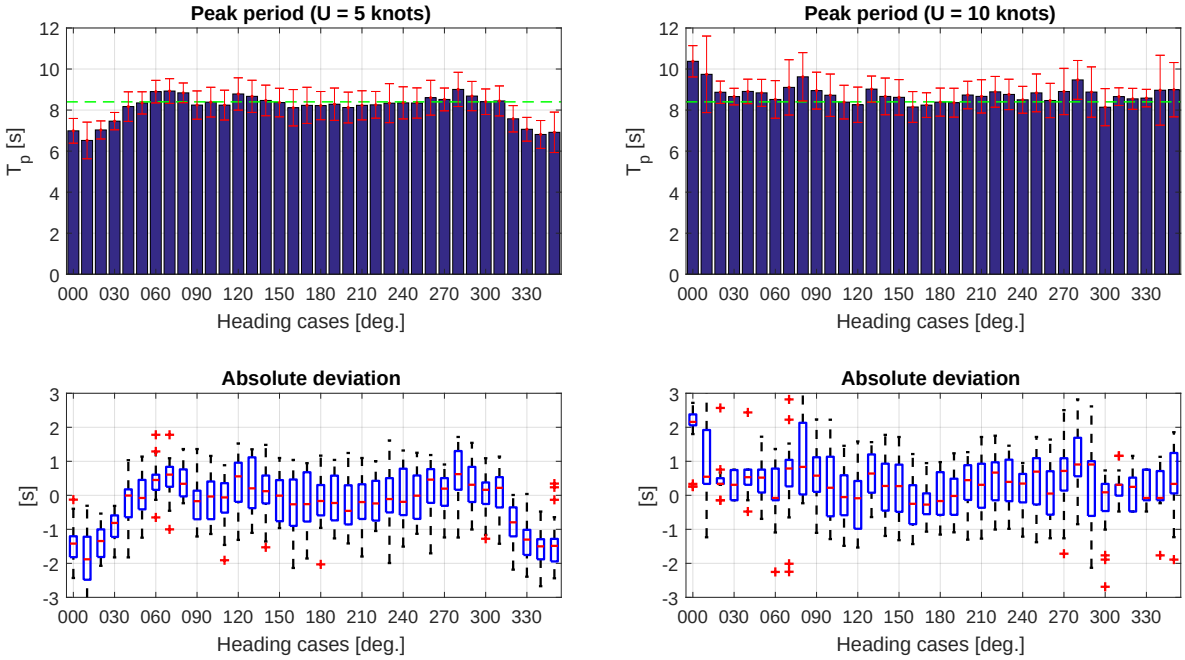

Figure 8: Upper plots: Estimates of **peak period** for all subcases (headings) of cases A (left-hand side) and B (right-hand side) with the true value indicated by the green dashed line. Lower plots: Deviations between estimates and true value shown as box plots; info is given in the caption of Fig. 6.

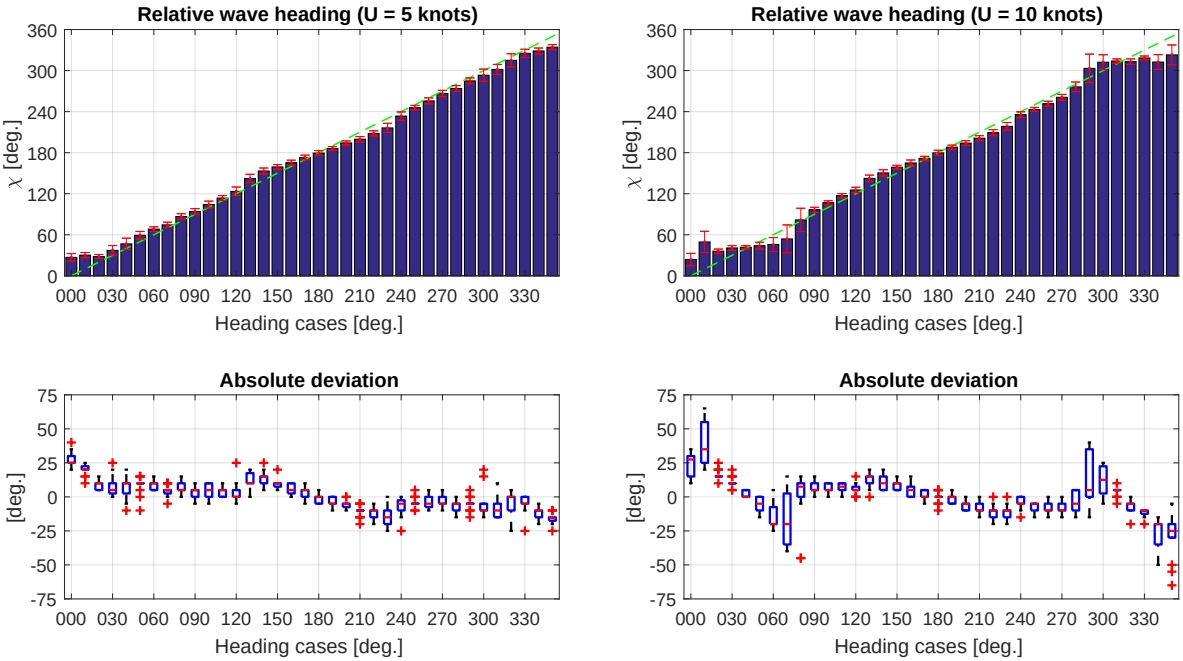

Figure 9: Upper plots: Estimates of (mean) **relative wave heading** for all subcases (headings) of cases A (left-hand side) and B (right-hand side) with the true value indicated by the green dashed line. Lower plots: Deviations between estimates and true value shown as box plots; info is given in the caption of Fig. 6.

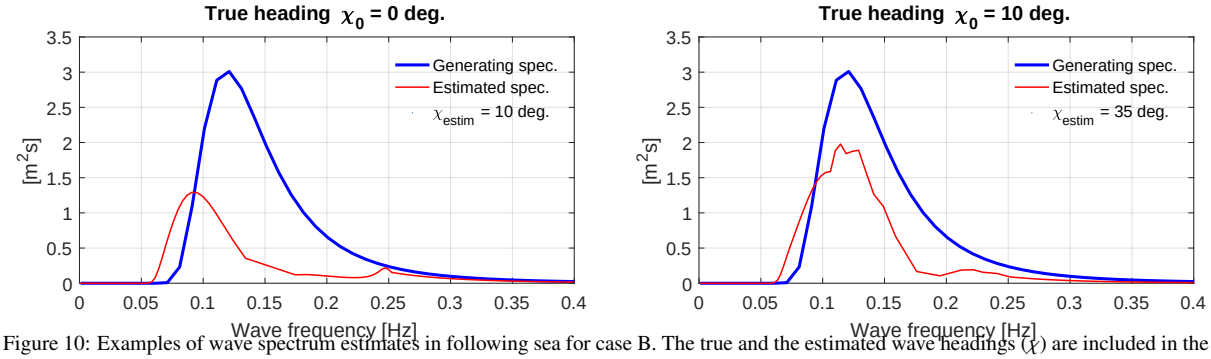

Figure 10: Examples of wave spectrum estimates in following sea for case B. The true and the estimated wave headings (χ) are included in the plot titles and legends, respectively.

any other estimation technique reported in the literature; of course also for cases without forward speed as explained by e.g. Mas-Soler et al. [26]. Generally, the underestimation reduces as the wave period increases, which is a benefit to the wave buoy analogy considering the more severe wave scenarios.

As reported above, the most significant inaccuracies of the estimates occur in strict following sea conditions (stern waves). Two specific outcomes of wave spectrum estimates are shown in Figure 10 for $U = 10$ knots (case B) at $\chi_0 = 10$ deg. $\chi_0 = 10$ deg. true wave headings; noting that the specific spectrum estimates are quite representative for the remaining estimates at the two headings (including $\chi = 350$ deg.); and applies also to the other vessel speed $U = 5$ knots (case A).

Efforts have tried to find the reason for the reduced agreement in stern waves but no clear answer has been found. One plausible explanation could be related to the 1-to-3 relationship, i.e. the Doppler Shift, for following waves, but - interestingly - very similar findings (not shown herein) apply for a situation without advance speed. Not to mention that the 1-to-3 relationship is introduced also at the other headings in following sea conditions, notably $\chi = 20 - 50$ deg., where the esti-

mates are as expected. It is therefore more likely that inaccuracies exist because of the actual hydrodynamic behaviour of the specific vessel, governed by hull geometry*, when it is exposed to stern waves (with or without advance speed), but investigations in this regard are left for future work.

Case C

In the last test case, C ($U = 10$ knots), swells and wind seas occur at the same time, making the wave spectrum double-peaked. The entire set of statistical plots is included in Figure 11 showing average and median values, including variation, of significant wave height estimates (upper left plot-pair), peak period estimates of swell (upper right plot-pair), peak period estimates of wind sea (lower left plot-pair), and wave heading estimates (lower right plot-pair), respectively. The statistics reveal somewhat similar findings, as were observed in the previous cases (A and B), but generally with a lower agreement between the estimates and the corresponding true values, and substantially larger variation around the average values (and medians). An exception is however the wave heading estimates which are just as good in this case; or in some subcases tending to be even better. It is noteworthy that at true headings $\chi_0 = 0$ deg. and $\chi_0 = 10$ deg., a few estimates are introduced with negative sign. That is, if the particular estimates were, say, 350 deg. the statistics are based on -10 deg. Some additional points to note from the plots are the following: The significant wave height is for all cases, except at wave headings slightly behind beam, lower than the true values, which is a result of the filtering characteristic of the ship in waves. The "inconsistent" result at headings just behind beam is not easily explained since it is not (necessarily) a result of fully correct spectrum estimates, which will be presented further below. The statistics concerning the peak periods of the swell and wind sea parts show an acceptable agreement, although the results are associated with rather large scatter. Moreover, it appears that at headings behind beam the peak periods are estimated closer together; i.e. the peak period of swell is too low and that of wind sea is too high. This observation is realised because the actual spectrum estimates are more blurred with a difficulty to distinctly detect (correctly) the two peaks of the wave system.

The findings mentioned above can be studied/confirmed by inspecting some of the actual spectrum estimates. Thus, for (true) wave headings $\chi_0 = 60$ deg. and $\chi_0 = 180$ deg. all 20 sets of realisations are included in Figure 12. Generally, the plots show a reasonable agreement between the spectrum estimates and the corresponding (generating) spectrum, capturing the most important part of the wave energy distribution. However, it is clear that the spectrum estimates are not as good as the findings were for cases A and B; notably problems occur for some of the 'behind-beam' sea conditions (around $\chi_0 = 60 - 90$ deg.) to detect the two individual peaks of the generating spectrum. It is also evident that the high-frequency part of the (true) wave energy distribution is not estimated correctly, which is a result of the filtering characteristic of the ship in waves.

5.2. Imperfect transfer functions

In this subsection, an *imperfect* set of motion transfer functions for the wave estimation process is imposed. More precisely, the transfer functions are calculated for a changed loading condition of the vessel, as "incomplete" knowledge is introduced simply by doing the calculations using as draught, $T_{new} = 1.1 \cdot T_0$, as displacement, $\Delta_{new} = 1.1 \cdot \Delta_0$, and as transverse metacentric height, $GM_{T,new} = 0.9 \cdot GM_{T,0}$, where the 0-index relates to the original parameter values seen in Table 1. It must be emphasised, however, that the new set of transfer functions is used only in the wave estimation part, while the time history simulations are made using the original set of motion transfer functions, based on the input in Table 1. Otherwise, the operational conditions, including wave system and vessel speed, are exactly as case B, studied in the previous subsection, see also Table 2.

The statistical outcomes of the entire set of spectrum estimates are presented in Figure 13. Indeed, the plots show that the estimates are still good, and by comparison to the right-hand side plots in Figures 6-9 the differences are barely visible. Basically, there are two (interrelated) ways to interpret this finding: 1) The estimation procedure is robust to changes in the applied motion transfer functions; 2) The particular example ship does not behave (very) differently when its loading condition is changed (slightly); or, strictly speaking, the calculated transfer functions [23, 24] exhibit little sensitivity to a change in the input parameters. Making a note here that, obviously, an estimation procedure cannot be robust/reliable if the used motion transfer functions are significantly off relative to the vessel's real hydrodynamic behaviour. However, it should be clear that the more (mathematically) complex the estimation procedure is, the more sensitive its results/estimates will be to changes.

*At this point, the particular set of motion transfer functions obviously plays a significant role.

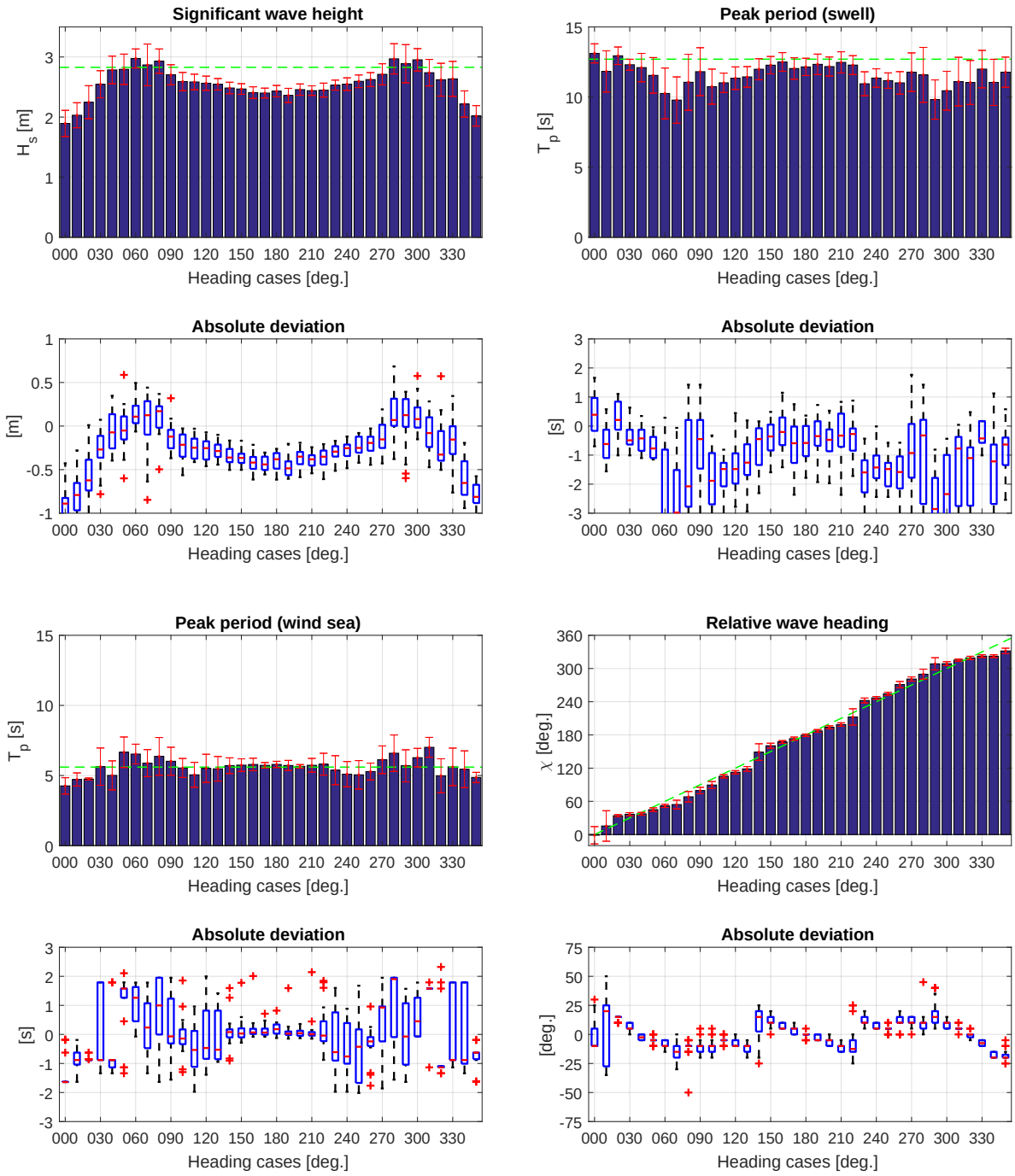

Figure 11: Estimates and deviations of significant wave height, peak periods for wind sea and swell, and relative wave heading, respectively, for all subcases (headings) of cases C with the true value indicated by the green dashed line. Deviations between estimates and true value shown as box plots. On each box, the central mark is the median, and the upper and lower edges of the box are the 25th and 75th percentiles, respectively. The whiskers extend to the most extreme data points which the algorithm considers not to be outliers, and the outliers are plotted individually.

The findings for the imperfect set of motion transfer functions should actually be viewed in a wider perspective than merely as indications of robustness; either it be of the estimation procedure itself, or whether it

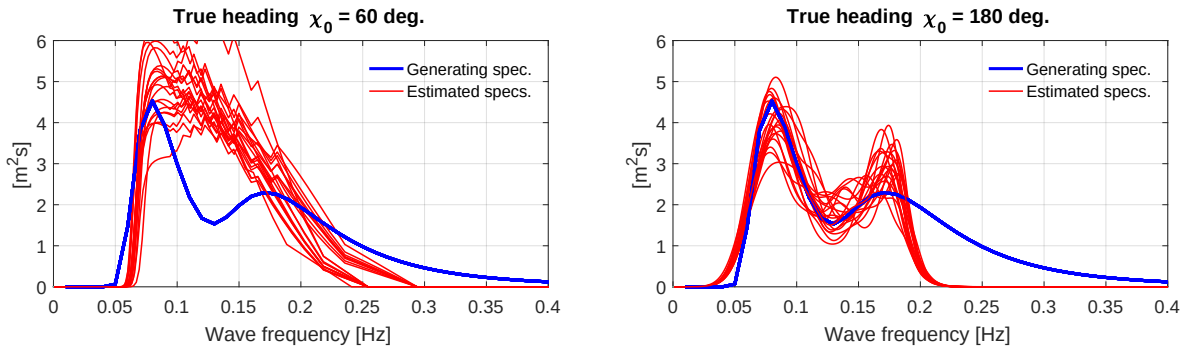

Figure 12: The entire set of wave spectrum estimates (total of 20) for headings χ_0 = 60 deg. and χ_0 = 180 deg. as the left- and right-hand side plots, respectively. The estimated wave headings were, in most cases, close to the true values (see Fig. 11).

means that the particular vessel and its associated hydrodynamic behaviour, represented by its motion transfer functions, exhibits little sensitivity to variations in the hull geometry and/or loading condition. Rather the key point is that, in real-case applications, it is useful to provide sea state estimates where an uncertainty measure, i.e. a "likeliness", is associated to the actual spectrum estimate, or to the corresponding integrated wave parameters. Means to accomplish this has (conceptually) been discussed in the literature [e.g. 5, 27, 28] and a deeper discussion of the means is beyond the scope of the present article. Instead, it suffices to say that probabilistic calculations in this respect will require *several* sea state estimates - for the very same condition, i.e governed by the exact same set of measurements, but using different sets of motion transfer function, where the input parameters are changed. Obviously, this means that the computational efficiency of the sea state estimation algorithm(s) must be very high. Indeed, this is so for the presented estimation procedure, since it is possible to obtain estimates in about 2-3 seconds*, all parts included and also the cross spectral analysis of the time history recordings. And, this calculation time is without doing anything to speed-up the computation or, in other ways, optimise for computational speed. Merely, the efficiency is a consequence of the brute-force approach, which the presented estimation procedure relies upon.

6. Conclusions and further work

It has been shown that the estimation procedure performs well and makes accurate prediction of the on-site sea state; this goes for the integrated wave parameters but also for the more 'delicate' frequency-wise distribution of wave energy, including the mean wave direction (relative heading). In this respect, the present *brute-force wave estimation procedure* has a performance comparable to many of the other shipboard estimation techniques relying on the wave buoy analogy. However, the computational efficiency of the present procedure is significantly improved with estimation speed in the order of a few seconds in contrast to minutes for the other well-tested estimation procedures based on Bayesian modelling or parametric optimisation. On the first hand, this makes the present procedure useful for realtime onboard control and decision support tools, where computational efficiency is vital. Secondly, the high computational speed means that it will be possible to integrate, in realtime, probabilistic calculations directly in the sea state estimation computations; something that cannot be made with other estimation techniques as they require too long computational time for the single spectrum estimates.

In the future, important and suggested work on the presented estimation procedure may be considering points on the following list, which by no means is exhaustive and does not necessarily include (sub)work already mentioned in the main text:

- Application to experimental data, including model-scale and full-scale, where motion measurements obtained on various types of ships (without and with advance speed) are analysed.

- Sensitivity studies taking many forms to examine, for instance, the influence of spectrum discretisation used in the cross spectral analysis; or to examine if certain response combinations will provide better spectrum estimates than others, depending on the operational and/or the wave conditions.

*Intel(R) Core(TM) i7-4600U CPU @ 2.10GHz

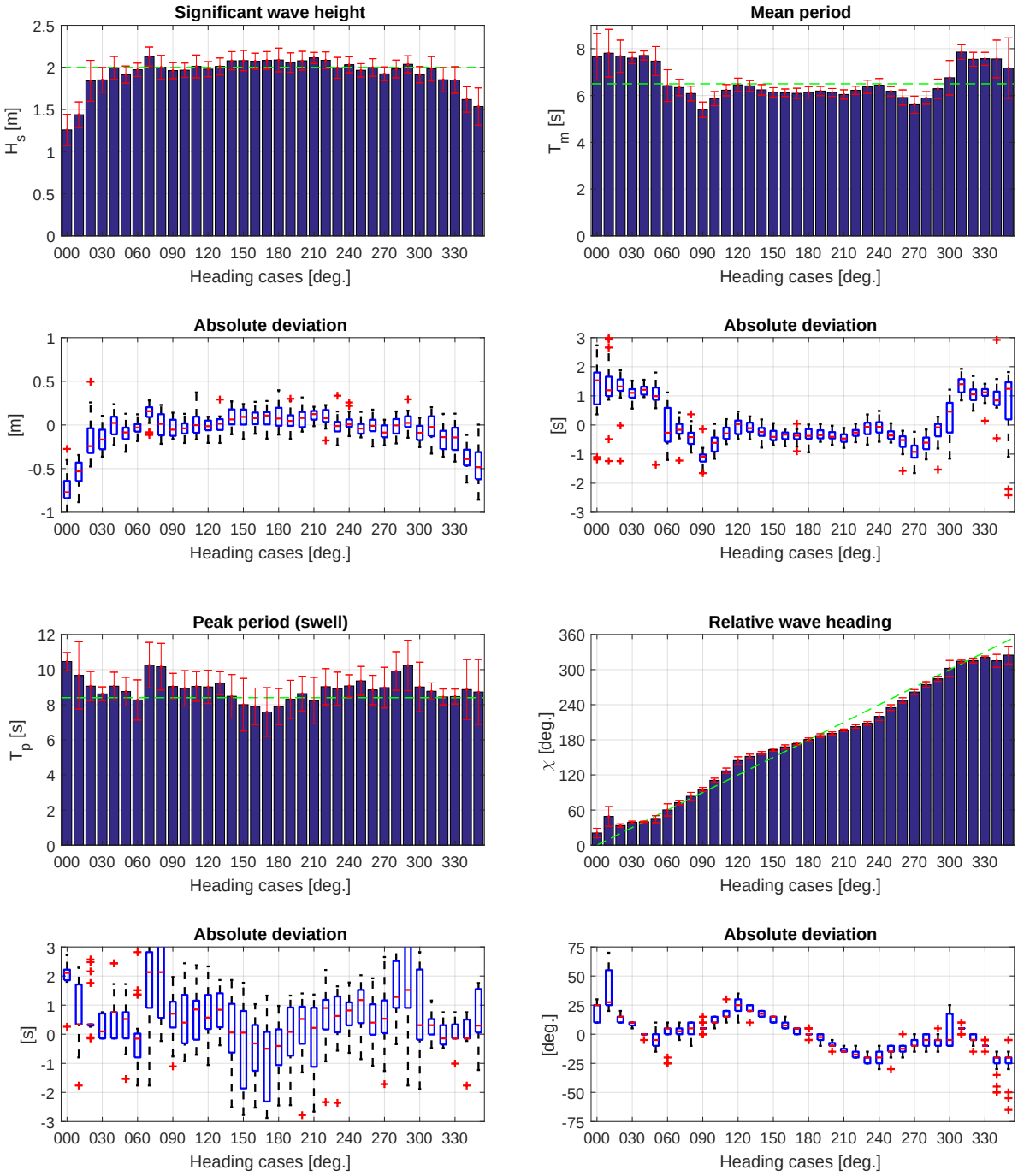

Figure 13: Estimates and deviations of significant wave height, mean periods, peak period, and relative wave heading, respectively, for all subcases (headings) of cases B using an imperfect set of motion transfer functions.

- To have the estimation procedure optimised for computational speed.
- Is it possible to extend the brute-force approach to work for wave systems composed by subsystems from different (mean) directions?

Acknowledgement

The first author would like to acknowledge his long-time colleague and friend Professor Emeritus Jørgen Juncher Jensen. It is interesting that Jørgen many years ago initiated a study introducing an (unpublished) idea for sea state estimation somewhat in line with the brute-force solution presented in this article.

This work was supported by the Research Council of Norway through the Centres of Excellence funding scheme, project number 223254 NTNU AMOS.

References

[1] M. Ludvigsen, A. Sørensen, Towards integrated autonomous underwater operations for ocean mapping and monitoring, Annual Reviews in Control 42 (2016) 145–157.

[2] T. Perez, Ship Seakeeping Operability, Motion Control, and Autonomy - A Bayesian Perspective, IFAC-PapersOnLine 48-16 (2015) 217–222.

[3] R. Veal, M. Tsimplis, The integration of unmanned ships into the lex maritima, Lloyd's Maritime & Commercial Law Quarterly (in press) .

[4] U. D. Nielsen, J. J. Jensen, A novel approach for navigational guidance of ships using onboard monitoring systems, Ocean Engineering 38 (2011) 444–455.

[5] U. D. Nielsen, Z. Lajic, J. J. Jensen, Towards fault-tolerant decision support systems for ship operator guidance, Reliability Engineering and System Safety 104 (2012) 1–14.

[6] U. D. Nielsen, A. H. Brodtkorb, J. J. Jensen, Response predictions using the observed autocorrelaton function, Marine Structures (under review) .

[7] T. Iseki, K. Ohtsu, Bayesian estimation of directional wave spectra based on ship motions, Control Engineering Practice 8 (2000) 215–219.

[8] E. A. Tannuri, J. V. Sparano, A. N. Simos, J. J. D. Cruz, Estimating directional wave spectrum based on stationary ship motion measurements, Applied Ocean Research 25 (2003) 243–261.

[9] R. Pascoal, C. G. Soares, A. J. Sørensen, Ocean Wave Spectral Estimation Using Vessel Wave Frequency Motions, Journal of Offshore Mechanics and Arctic Engineering 129 (2007) 90–96.

[10] R. Pascoal, L. P. Perera, C. G. Soares, Estimation of Directional Sea Spectra from Ship Motions in Sea Trials, Ocean Engineering 132 (2017) 126–137.

[11] U. D. Nielsen, Estimations of on-site directional wave spectra from measured ship responses, Marine Structures 19 (2006) 33–69.

[12] U. D. Nielsen, Introducing two hyperparameters in Bayesian estimation of wave spectra, Probabilistic Engineering Mechanics 23 (2008) 84–94.

[13] U. D. Nielsen, A concise account of techniques available for shipboard sea state estimation, Ocean Engineering 129 (2017) 352–362.

[14] A. H. Brodtkorb, U. D. Nielsen, A. J. Sørensen, Sea State Estimation Using Vessel Response in Dynamic Positioning, Applied Ocean Research (accepted for publication) .

[15] R. Pascoal, C. G. Soares, Non-parametric wave spectral estimation using vessel motions, Applied Ocean Research 30 (2008) 46–53.

[16] U. D. Nielsen, The wave buoy analogy - estimating high-frequency wave excitations, Applied Ocean Research 30 (2008) 100–106.

[17] N. Montazeri, U. D. Nielsen, J. J. Jensen, Estimation of wind sea and swell using shipboard measurements - A refined parametric modelling approach, Applied Ocean Research 54 (2016) 73–86.

[18] R. Bhattacharyya, Dynamics of Marine Vehicles, John Wiley & Sons, 1978.

[19] R. Beck, W. Cummins, J. Dalzell, P. Mandel, W. Webster, Vol. III: Motions in Waves and Controllability, in: E. Lewis (Ed.), Principles of Naval Architecture, Second Revision, SNAME, 1–188, 1989.

[20] J. Journée, W. Massie, Offshore Hydromechanics, lecture notes in course offered at TU Delft, 2001.

[21] U. D. Nielsen, Transformation of a wave energy spectrum from encounter to absolute domain when observing from an advancing ship, Applied Ocean Research (submitted for posible publication) .

[22] U. D. Nielsen, D. C. Stredulinksy, Sea state estimation from an advancing ship - A comparative study using sea trial data, Applied Ocean Research 34 (2012) 33–44.

[23] J. J. Jensen, A. E. Mansour, A. S. Olsen, Estimation of ship motions using closed-form expressions, Ocean Engineering 31 (2004) 61–85.

[24] A. Mansour, J. Jensen, A. Olsen, Fast Evaluation of the Reliablity of Container Securing Arrangements, in: Proceedings of PRADS'04, Travemünde, Germany, 577–585, 2004.

[25] J. J. Jensen, J. Capul, Extreme response predictions for jack-up units in second order stochastic waves by FORM, Probabilistic Engineering Mechanics 21 (2006) 330–338.

[26] J. Mas-Soler, A. N. Simos, E. A. Tannuri, Estimating on-site wave spectra from the motions of a semi-submersible platform: An assessment based on model scale results, Ocean Engineering (under review) .

[27] T. Iseki, An improved stochastic modeling for bayesian wave estimation, in: Proc. of OMAE 2012, ASME, Rio de Janeiro, Brazil, 2012.

[28] I. M. V. Andersen, G. Storhaug, Dynamic Selection of Ship Responses for Estimation of on-site Directional Wave Spectra , in: Proc. 31st OMAE, Rio de Janeiro, Brazil, 2012.